Electrochemical investigation of oxygen reduction reaction on La$_{0.6}$Sr$_{0.4}$Co$_{0.2}$Fe$_{0.8}$O$_{3-\delta}$ cathodes deposited by Electrostatic Spray Deposition

Daniel Marinha*, Laurent Dessemond, Elisabeth Djurado

LEPMI, UMR 5279, CNRS, Grenoble INP, Université de Savoie, Université Joseph Fourier, BP75, 38402 Saint Martin d'Hères Cedex, France

ARTICLE INFO

ABSTRACT

The oxygen reduction reaction of La$_{0.6}$Sr$_{0.4}$Co$_{0.2}$Fe$_{0.8}$O$_{3-\delta}$ (LSCF) cathodes deposited by Electrostatic Spray Deposition (ESD) onto dense Ce$_{0.9}$Gd$_{0.1}$O$_{2-\delta}$ (CGO) electrolytes was characterized by means of impedance spectroscopy measurements. Three cathodes with distinct morphologies and surface areas were prepared. Impedance measurements were performed at temperatures between 450 and 600 °C, at 50 °C steps. At each temperature, impedance measurements were performed at five different oxygen partial pressures (p_{O_2}), between $\sim 10^{-4}$ and 1 atm. This approach permitted a systematic evaluation of the influence of microstructure, temperature and p_{O_2} on the electrochemical behavior of the cathodes. Up to three contributions were identified in the high (*HF*), medium (*MF*) and low frequency (*LF*) ranges. The *LF* response displays the strongest dependence on oxygen partial pressure with corresponding resistance and capacitance values increasing with decreasing p_{O_2}. Contrarily, the resistance associated with the *HF* response remained practically constant with changing p_{O_2}, while a slight dependence was found for the *MF* response. The analysis provides support to the assignment of the *HF*, *MF* and *LF* contributions respectively to the ionic transfer at the cathode/electrolyte interface, bulk diffusion of oxygen species and oxygen surface exchange at $p_{O_2} > 10^{-2}$ atm. At lower p_{O_2}, an increasing contribution of oxygen gas-phase diffusion with temperature, evidenced by the *LF* response, was suggested.

© 2011 Elsevier B.V. All rights reserved.

1. Introduction

La$_{1-x}$Sr$_x$Co$_{1-y}$Fe$_y$O$_{3-\delta}$ (LSCF) has been widely studied as a mixed ionic-electronic conductor (MIEC) cathode. A combination of high catalytic activity and transport properties result in lower polarization resistances, R_{pol}, values at lower temperatures than those reported for La$_{1-x}$Sr$_x$MnO$_3$ (LSM) [1–3]. LSCF is known to react with YSZ electrolytes around 900 °C to form insulating phases at the cathode/electrolyte interface [4,5]. Instead, Ce$_{0.9}$Gd$_{0.1}$O$_{2-\delta}$ (CGO) electrolytes have been used with no known adverse reactions under typical operating conditions [6,7]. Despite of the electronic leakage observed under reducing atmospheres, CGO is nonetheless considered a suitable electrolyte for intermediate temperature (IT)-SOFCs [8].

Electrostatic Spray Deposition (ESD) technique has been previously used to deposit SOFC cathodes [9–11]. In ESD a precursor solution is pumped through a metallic nozzle which is placed beneath a heated substrate. An electrical field is applied between the nozzle and the substrate, generating electrohydrodynamic forces that atomize the precursor solution. The aerosol is composed of finely dispersed droplets which follow the electrical field towards the substrate, where they deposit. The final microstructure of the film depends directly on the size of the droplets which can be tuned by changing deposition parameters such as the substrate temperature, the solution flow rate and the nozzle-to-substrate distance [9,12,13].

The behavior of LSCF films prepared by ESD with different microstructural features by means of impedance spectroscopy has been previously analyzed in air [14]. A strong relationship between R_{pol} values and oxygen exchange at the cathode/gas interface was found, with values varying between 0.8 Ω cm^2 and 6.3 Ω cm^2 at 600 °C. This is representative of the even greater dispersion of R_{pol} values reported in the literature [10,15–21], originating from differences in film morphology and current collection methods. It has been shown that larger cathode surface areas result in lower R_{pol} values [22].

In order to improve performance it is important to identify the elementary steps involved in the cathodic reaction, which are rate-limiting and under which conditions. A common procedure is to analyze the behavior of R_{pol}, as a function of temperature. However, further detail may be obtained by performing impedance measurements versus the oxygen partial pressure, p_{O_2}. Indeed, the exponent n, deduced from the power law dependence of R_{pol} versus p_{O_2} according to $R_{pol} = C \times p_{O_2}^{-n}$, where C is a constant, provides information about the nature of the reaction and of the species involved in the operating electrode [15,23–25]. Many

* Corresponding author. Tel.: +351 917 146 461; fax: +33 476826777.
E-mail address: danielmarinha@gmail.com (D. Marinha).

Table 1
Summary of the sample deposition conditions: substrate temperature, T; solution flow rate, Q; nozzle-to-substrate distance, d; deposition time, t; voltage, V and precursor solution.

Microstructure	Sample	$T/°C$	$Q/mL\,h^{-1}$	d/mm	t/h	V/kV	Precursor solution
Dense	1	300	1.59	30	1	9	A
Cracked	2	350	1.59	15	2	8	A
Coral	3	350	1.0	35	3	10	B

impedance studies have been dedicated to the performance of LSCF-based cathodes in air [10,26–36], and some performed under varying p_{O_2} [15,24,28,34,37,38]. Amongst these, however, a systematic variation of the measuring conditions for different cathode microstructures is still lacking.

In this study, a systematic investigation of the oxygen reduction reaction on $La_{0.6}Sr_{0.4}Co_{0.2}Fe_{0.8}O_{3-\delta}$ cathodes under varying temperature and p_{O_2}. This composition is a compromise between optimal transport behavior, catalytic properties of LSCF and thermo-mechanical stability regarding CGO [7,39]. Impedance measurements were carried out from 450 to 600 °C under oxygen partial pressures ranging from $\sim 10^{-4}$ to 1 atm. Dense uniform films can be regarded as model electrodes of well-defined geometry to suggest an oxygen reduction mechanism, whereas the behavior of standard cathodes is necessarily different due to their porous nature. The electrochemical characterization was performed on three representative cathodes with distinct morphologies to further evaluate the role of the electrode microstructure.

2. Materials and methods

2.1. Sample preparation

LSCF films were deposited on homemade CGO substrates using a vertical ESD process [9]. CGO pellets were cylindrical in shape, with 18 mm in diameter and 1.2 mm in thickness.

Precursor salts solution was prepared by weighing $La(NO_3)_3\cdot6H_2O$ (Prolabo, 99.99%), $SrCl_2\cdot6H_2O$ (Strem Chemicals, 99%), $Co(NO_3)_2\cdot6H_2O$ (Sigma–Aldrich, 99.999%) and $Fe(NO_3)_2\cdot9H_2O$ (Sigma–Aldrich, 99.99%) salts in adequate amounts to obtain the $La_{0.6}Sr_{0.4}Co_{0.2}Fe_{0.8}O_{3-\delta}$ stoichiometry. Two separate solutions were prepared by mixing salts in ethanol (C_2H_5OH, 99.9%; Prolabo) and diethylene glycol monobutyl ether, also known as butyl carbitol ($CH_3(CH_2)_3OCH_2CH_2OCH_2CH_2OH$, 99+%; Acros Organics 99+%) with a 1:2 volume ratio, respectively, (Solution A) and in ethanol and distilled water with a 1:4 volume ratio, respectively (Solution B). Both solutions had a total salt concentration of $0.02\,mol\,L^{-1}$. The deposition conditions (Table 1) were selected in order to obtain three different morphologies. Resulting films were annealed at 900 °C for 2 h in air.

Microstructures of the deposited films were studied using a field-emission gun scanning electron microscope, FEG-SEM (ZEISS Ultra 55) energy dispersive X-ray analyzer (EDX).

2.2. Electrochemical characterization

Impedance measurements were performed in a three-electrode configuration at open circuit potential (OCP), using the LSCF film as working electrode (WE). Platinum paste (Metalor, No. 6982) was painted onto the symmetrically opposite side of the CGO pellet to serve as the counter electrode (CE). The reference electrode was painted along the circumference of the electrolyte pellet. WE and CE areas were kept constant at $\sim 0.5\,cm^2$ and positioned at the center of the CGO pellet, so as to avoid possible interference between electrodes during measurements. Platinum paste was annealed at 800 °C for 1 h in air. Platinum grids (Heraeus, mesh 3600) were mechanically pressed against the WE and CE and used as electrical
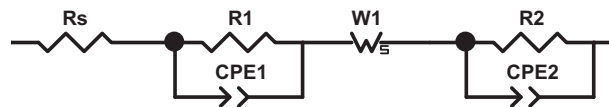
current collectors. Uniaxial pressing was used to flatten platinum grids. Platinum wires (Ögussa, $\phi_{ext} = 0.2$ mm) were used to connect all electrodes to the external electric circuit.

Electrochemical characterization of LSCF films was carried out between 450 and 600 °C. Oxygen partial pressure was varied between 1 and $\sim 10^{-4}$ atm using a homemade oxygen pump-gauge system based on stabilized zirconia. The total gas flow was fixed at $5\,L\,h^{-1}$. Impedance measurements were performed using a Solartron (SI 1280B) potentiostat/galvanostat frequency response analyzer with frequencies ranging from 0.01 Hz to 20 KHz (13 steps per decade). Amplitude of 10 mV for the measuring sinusoidal voltage was chosen to ensure the linearity of the electrical response. All impedance diagrams have been normalized to the WE area.

In this work, an equivalent electric circuit (Fig. 1) was used to fit the experimental impedance plots. The R_s, R1, W and R2 elements correspond to a series resistance, R_s, high frequency, HF, medium frequency, MF, and low frequency, LF, features, respectively. Constant phase elements, CPE, used in combination with HF and LF features were used instead of pure capacitances as a better approximation of the non-ideal behavior of impedance semicircles depressed below the real axis in the Nyquist plane. The impedance of a CPE element is expressed by $Z_{CPE} = (Q(iw)^p)^{-1}$ where Q and p are fitting parameters and w is angular frequency. The value of the related capacitance, C, can be determined from the relationship $C = (R^{1-p}Q)^{1/p}$. Impedance diagrams were fitted to equivalent circuits using the ZView® software (Scribner Associates).

3. Results

3.1. Materials characterization

SEM micrographs reveal the morphological differences between the LSCF films, henceforth referred to as dense (Fig. 2a–c), cracked (Fig. 2d–f) and coral (Fig. 2g–i), based on the external structure of the films. At the nanometric scale, however, a similar morphology is observed across samples, consisting of homogeneously sized solid particles and internal pores. The dense film averages 1.5 μm in thickness, has well interconnected particles and is clearly much less porous than other samples. The large majority of available porosity is nanometric in size and enclosed within the film, thus limiting oxygen access to cathode. The cracked film is ~ 13 μm thick with ~ 1 μm wide gaps that cut across the film, reaching the electrolyte. These cracks considerably increase the surface area of the film relatively to the dense sample. The microstructure of the coral film yields an even larger surface area, with solid particles arranged in a highly ramified structure resembling oceanic corals. Surface area values were confirmed through a detailed microstructure analysis of similarly processed LSCF films, using a 3D image reconstructed from FIB sectioned areas (submitted paper). A relatively dense
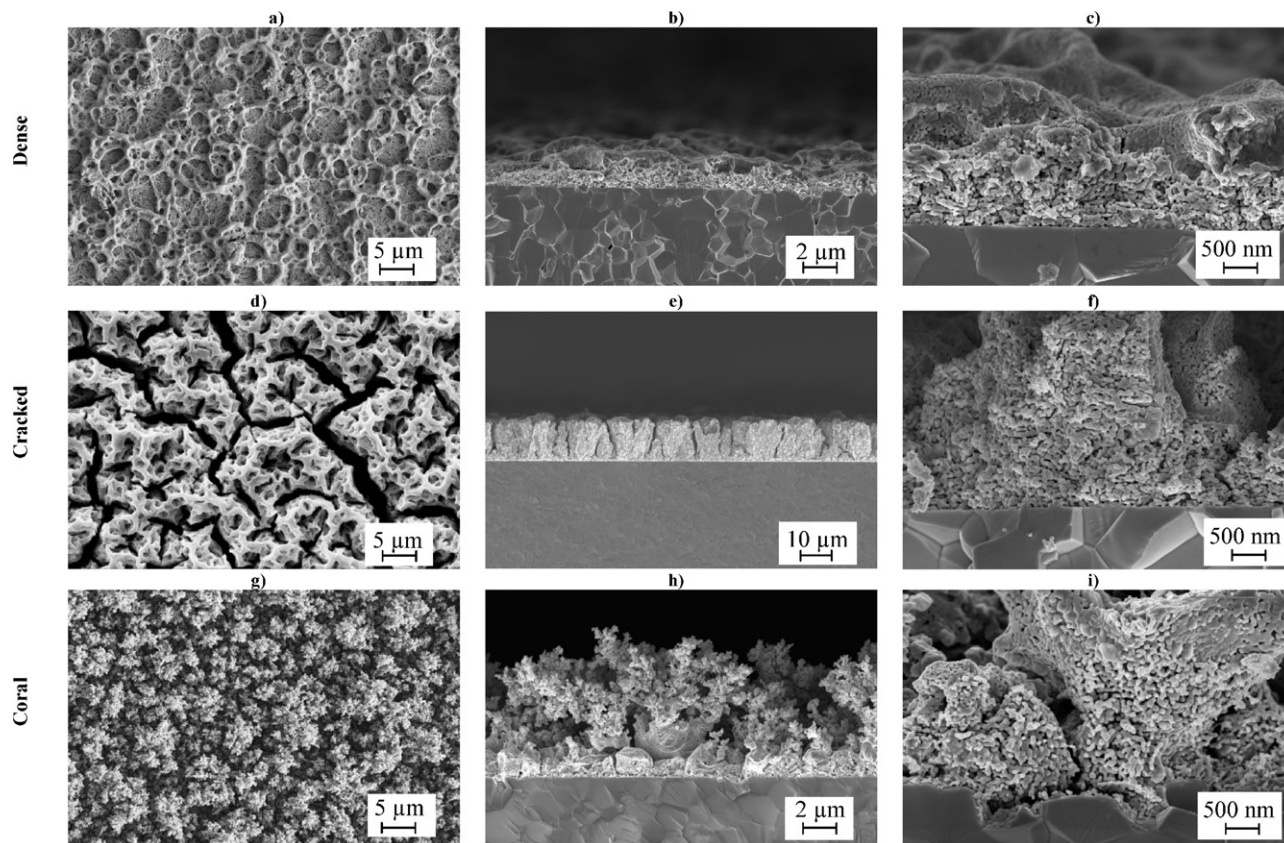

Fig. 1. Equivalent electric circuit used in modeling experimental impedance diagrams.

Fig. 2. SEM micrographs of surface and cross-section views of dense (a–c), cracked (d–f) and coral (g–i) films.

intermediate layer at the cathode/electrolyte interface is visible in all samples, varying from 0.5 to 2 μm in thickness. Regardless of the microstructure of the film, no delamination was ever observed.

3.2. Electrochemical characterization

Typical impedance diagrams recorded at 450 °C in air are shown in Fig. 3. Overall shape is similar to those of LSCF-based electrodes in the same temperature range [2,15,28,40,41]. The series resistance, R_s, defined as the high frequency intercept of the electrode characteristic on the real axis, is expected to be exclusively related to the ohmic resistance corresponding to the electrolyte volume between

WE and CE in a three-electrode configuration. The total polarization resistance, R_{pol}, is defined as the difference between the intersections of low and high frequency limits of the electrode characteristic with the real axis in the Nyquist plane. Up to three elementary contributions, referred to as high (HF), medium (MF) and low frequency (LF), can be identified in impedance diagrams performed between 450 and 600 °C at OCP. In the conditions of Fig. 3, the apex frequency values (corresponding to the minimum of the imaginary part of the measured impedance) for HF, MF and LF contributions in all electrodes were 184.6, 8.9 and 0.8 Hz (average values), respectively. It is worth noting that the frequency distribution of the electrode characteristic is independent of film morphology, indicating that similar elementary steps are involved in the reaction mechanism. Regardless of the oxygen partial pressure, the largest contribution to the polarization resistance comes from the LF response of the electrode characteristic.

R_{pol} is a decreasing function of the measuring temperature (Fig. 4). R_{pol} values at 600 °C of 1.2, 1.6 and 9.5 Ω cm² were determined for the cracked, dense and coral samples, respectively. Corresponding activation energy varies from 1 to 1.2 eV (Table 2), consistent with literature results (1.23–1.69 eV) for LSCF films deposited onto CGO electrolytes [10,16–19,28,34,42].
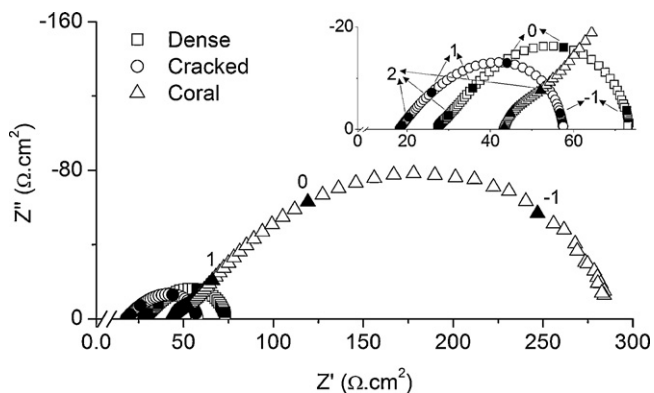

Fig. 3. Impedance diagrams recorded at 450 °C in air for all samples (OCP conditions). The numbers over the diagram indicate the logarithm of the measuring frequency.

Table 2
Activation energies of elementary steps and total polarization resistance values, in air.

Sample	E_a/eV			
	R_{HF}	R_{MF}	R_{LF}	R_{pol}
Dense	0.81	1.36	1.24	1.23
Cracked	–	1.32	0.87	1.00
Coral	1.33	0.78	1.24	1.19
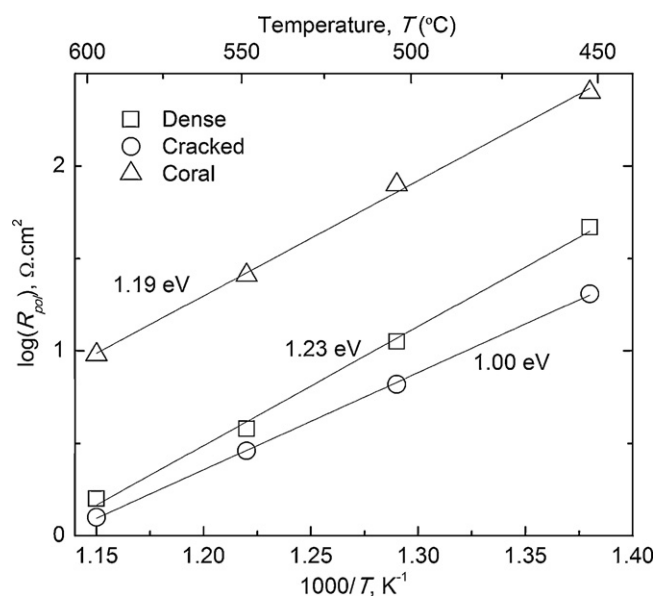
Fig. 4. Arrhenius plots of R_{pol} in air for dense, cracked and coral LSCF cathodes (OCP conditions).

Fig. 5. Arrhenius plots of R_{HF} as a function of p_{O_2}, for the coral cathode (OCP conditions).

Although the quality of the LSCF/CGO interface is similar for the three electrodes, R_s varies significantly in air (Fig. 3). This behavior is not thought to be due to microstructural differences between CGO pellets. Instead, it is related to constriction of current lines due to the discrete contacts provided by the metal mesh used as current collectors. This setup yields a heterogeneous current distribution within the cathode and consequently at the LSCF/CGO interface [43,44]. Such effects are exacerbated by large sheet resistance values, typical of thin films [38], as well as in films with otherwise interrupted current paths [45]. The higher R_s value observed for the dense and coral sample, as well as the anticipated high magnitude of the HF contribution [46,47], are in favor of this assumption. Moreover, R_s in dense and in coral samples was found to increase with decreasing oxygen partial pressure. However, the recorded variations were far smaller than those determined versus the electrode microstructure (not shown). Comparatively, the smoother surface of the cracked film improves the quality and number of contacts with the platinum mesh, and the bulkier nature of the cathode contributes to a homogeneous distribution of current lines, resulting in lower R_s values. This behavior further suggests a contribution of the electrode volume to R_s. It is worth mentioning that the recorded variation of the R_s versus the electrode morphology does not act upon the proposed description of the oxygen reduction mechanism on LSCF electrodes.

The HF response was only observed in dense and coral samples. Such a contribution is usually not observed in thicker LSCF layers [36,37] or when using an additional current collecting layer [38], in which case it may be either convoluted or even absent. Nevertheless, it is clearly evidenced in geometrically well-defined dense cathode films, with thicknesses in the sub-micrometric range [26,45,48]. In such cases, diffusion of oxygen is negligible and the HF contribution can be easily separated from the dominating surface exchange reaction occurring in the low frequency range. Consequently, the HF arc may be straightforwardly associated with ionic transfer between the electrode and the electrolyte.

Arrhenius plots of corresponding resistance, R_{HF}, with varying p_{O_2} reveals similar temperature dependences in both samples. Corresponding activation energy values varied between 0.9 eV and 1.2 eV (Fig. 5).

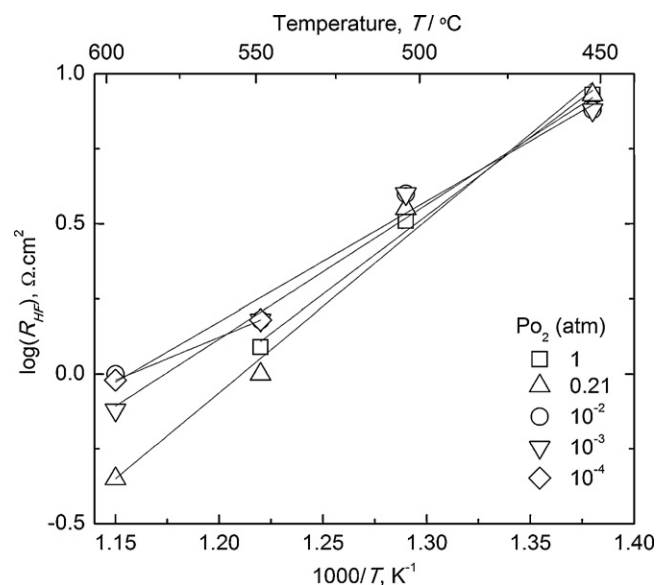Between 450 and 600 °C, R_{HF} displays a very weak dependence versus p_{O_2}, with maximum n values of 0.1–0.06 for the

dense and coral samples, respectively (Table 3). Similar exponent ($0.06 < n < 0.1$) and activation energy values (1.26 eV) have been reported by Escudero et al. [49] for $La_2NiO_{4+\delta}$ cathodes on YSZ between 600 and 800 °C. Higher n values were reported for $Sm_{0.2}Ce_{0.8}O_{1.9}$ ($n \sim 0.25$) [50] and for $PrBaCo_2O_{5+\delta}$ ($0.18 < n < 0.28$) [51] cathodes on samaria-doped ceria electrolytes at 800 and 900 °C, respectively. For all assemblies, the contribution of the electrode/electrolyte interface has been invoked.

If one refers to the apex frequency of the HF contribution, typical values, determined at 600 °C, within the experimental p_{O_2} variation, range between 27 Hz and 369 Hz for the dense cathode and between 38 Hz and 235 Hz for the coral cathode, in agreement with literature data [28,45]. This supports the assignment of this contribution to ionic transfer at the internal LSCF/CGO interface, in both electrodes. Another argument in favor of this assumption is the variation of the HF capacitance, C_{HF}, as functions of temperature and oxygen pressure [26,38,52–54]. In air, C_{HF} values vary between 10^{-3} and 10^{-4} F cm^2 and remain practically constant with temperature (Fig. 6). At fixed temperatures, this capacitance is a decreasing function of p_{O_2}. This behavior is associated with an interfacial capacitance coupled with charge transfer phenomena [55]. These values are too high for a pure double layer capacitance and may instead be related to stoichiometric changes occurring at the interface.

A Warburg element can be identified in the medium frequency range of the electrode characteristic, regardless of the p_{O_2} range or film morphology. In assuming a Warburg impedance [24,36], one can expect a bulk diffusion process, as is often considered [16,18,28,56,57]. In air, activation energies of 1.4, 1.3 and 0.8 eV were determined for dense, cracked and coral films. A large dispersion of activation energy values (0.64–1.93 eV) determined by

Table 3
Exponent n values for the p_{O_2} dependence of R_{HF} as a function of temperature in dense and coral cathodes.

$T/°C$	Sample	
	Dense	Coral
450	0.07	0
500	0.1	0.02
550	0.07	0.02
600	0	0.06

Fig. 6. C_{HF} versus p_{O_2} for the coral cathode.

Table 4
Activation energy, E_a, for R_{LF} as a function of p_{O_2}.

Sample	E_a/eV				
	1 atm	0.21 atm	10^{-2} atm	10^{-3} atm	10^{-4} atm
Dense	1.3	1.2	1.2	0.9	0.8
Cracked	1.2	1.0	1.3	1.2	0.5
Coral	1.5	1.2	1.6	1.3	0.9
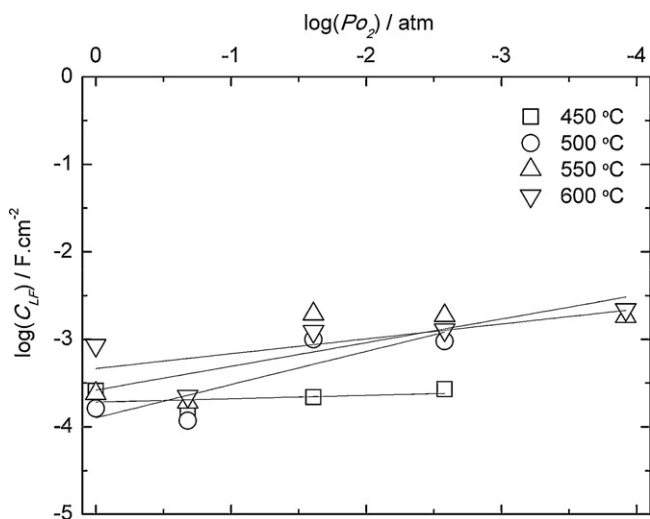
oxygen diffusion measurements studies in identical LSCF compositions is found in the literature [58–61]. Between 450 and 600 °C and for a given morphology, the corresponding activation energy remains practically unaffected by p_{O_2} (Fig. 7), indicating that the nature of the related process remains unchanged.

In the investigated range, a weak dependence of R_{MF} on p_{O_2} was observed ($0.02 \leq n \leq 0.23$), regardless of film morphology. For the dense cathode, R_{MF} remains nearly constant, in agreement with literature data on $La_{1-x}Sr_xCo_{0.2}Fe_{0.8}O_{3-\delta}$ dense electrodes with $0.1 < x < 0.3$ [37]. Similarly weak dependences have also been evidenced for $La_{0.58}Sr_{0.4}Co_{0.2}Fe_{0.8}O_{3-\delta}$ [57], $La_{0.8}Sr_{0.2}Co_{0.2}Fe_{0.8}O_{3-\delta}$ [28] and $La_{0.6}Sr_{0.4}Co_{0.8}Fe_{0.2}O_{3-\delta}$ [36] porous cathodes.

Results suggest that the concentration of oxygen vacancies, and thus the electrode oxygen deficiency, does not vary significantly within experimental conditions. According to the increase of the resistance related to the LF contribution in the electrode characteristic (see below), one can infer that the oxygen exchange rate is an increasing function of the oxygen partial pressure [56]. Accordingly, the effect of an increase in the concentration of oxygen vacancies with decreasing p_{O_2} [36] can be counterbalanced by a decrease in the exchange rate [62].

As expected from the contribution of the bulk pathway to the reaction mechanism, R_{MF} increases with electrode thickness. For

instance, R_{MF} increases fivefold between dense and coral samples at 600 °C (Fig. 7). But a direct correlation between both parameters is not straightforward. Indeed, similar resistance values were determined for dense and cracked samples in spite of different thicknesses. This can be related to the different surface areas of the investigated films. Assuming a homogeneous distribution of active sites for oxygen reduction along the cathode surface, then all electroactive regions are easily accessible to oxygen and the reaction will occur preferentially near the electrolyte interface where diffusion lengths are shorter [38,63]. This agrees with the existence of an effective electrode thickness corresponding to a fraction of the cathode layer involved in oxygen bulk transport [62,64], estimated to vary from 0.1 to 2 μm between 500 and 650 °C in LSCF samples with similar microstructures [63].

Regardless of film morphology, the single largest contribution to the electrode impedance originates from the LF process (Fig. 3). Moreover, this process is the most sensitive to changes in p_{O_2}. Activation energies of 1.2, 0.9 and 1.2 eV (Table 2) were determined in air for the dense, cracked and coral samples, respectively, in agreement with reported values for thin dense films (1.1–1.6 eV) of similar composition [26,48]. For all electrodes, the activation energy varies only slightly with the oxygen partial pressure down to 10^{-2} atm, after which point a decrease is observed (Fig. 8 and Table 4).

R_{LF} is a decreasing function of the oxygen pressure, regardless of film morphology. Moreover, a change in p_{O_2} dependence is evidenced between high ($p_{O_2} > 10^{-2}$ atm) and low ($p_{O_2} < 10^{-2}$ atm) ranges (Fig. 9). For the coral sample, this behavior was only confirmed above 500 °C because of very large impedance moduli at lower temperatures below 10^{-3} atm.

The above results underline the complexity of the oxygen reduction reaction mechanism. For $p_{O_2} > 10^{-2} atm$, the weak dependence of R_{LF} proves unambiguously that gas-phase mass transport is not limiting, since a reciprocal p_{O_2}-dependence would be expected (Table 5). This is corroborated by the practically
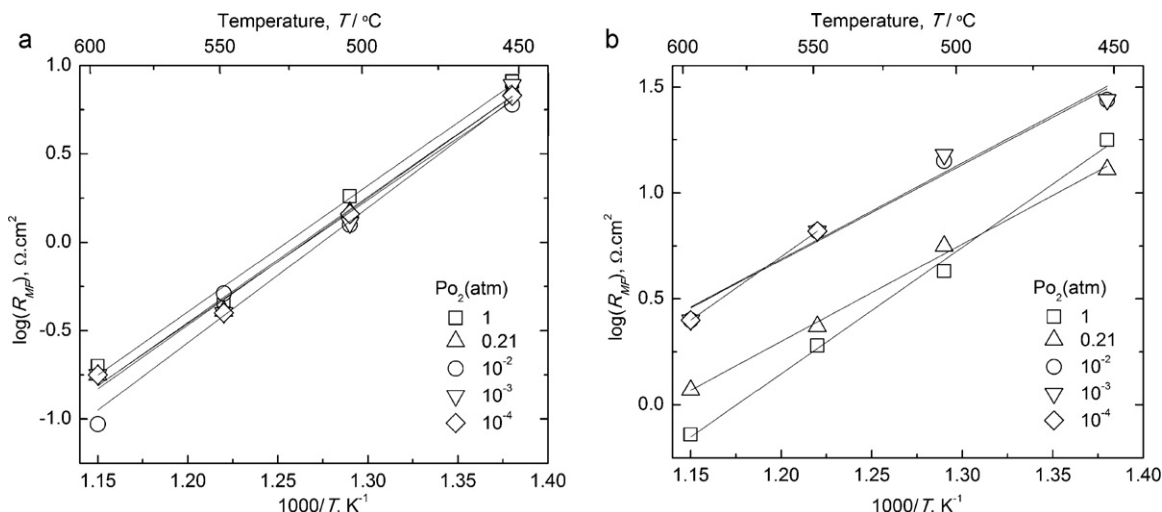

Fig. 7. Arrhenius plots of R_{MF} for dense (a) and coral (b) samples as functions of p_{O_2}.
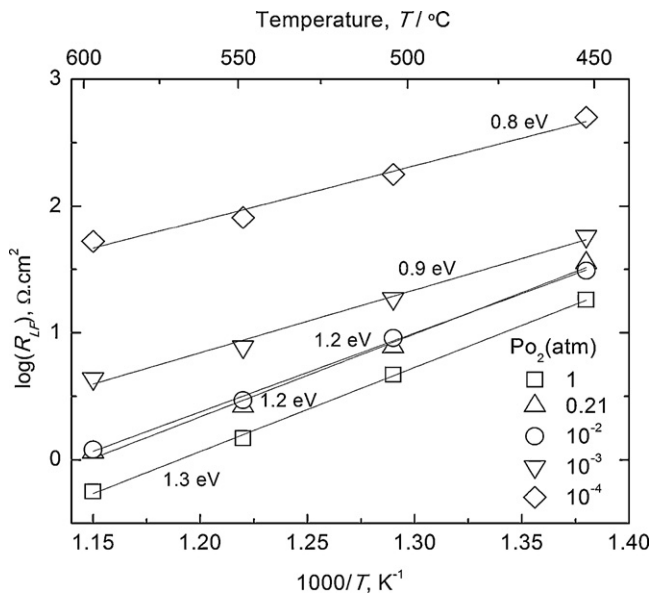
Fig. 8. Arrhenius plots of R_{LF} as a function of p_{O_2}, for dense cathode.

Fig. 10. C_{LF} versus p_{O_2} for the cracked cathode.

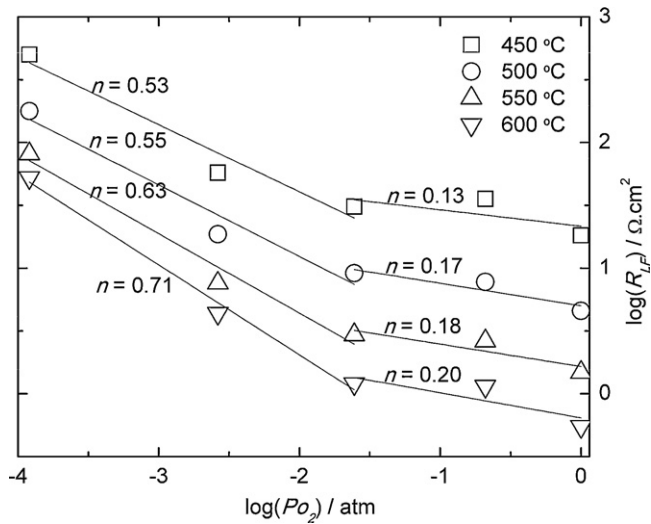Fig. 9. R_{LF} versus p_{O_2} for the dense cathode.
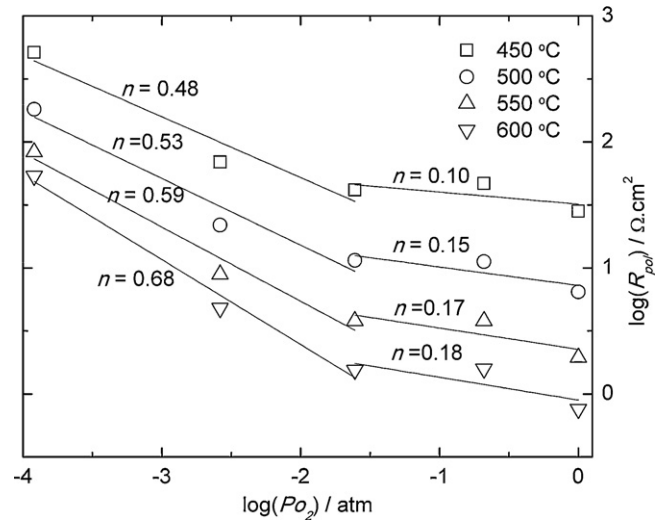
Fig. 11. R_{pol} versus p_{O_2} for the dense cathode.

constant values of the corresponding activation energy (Table 4). Furthermore, it demonstrates that such films can be used in rather weak oxygen partial pressure ($p_{O_2} \sim 10^{-2}$ atm) without severe performance losses, particularly at temperatures above 550 °C.

For all investigated electrodes, the capacitance associated with the LF response, C_{LF}, is a decreasing function of the oxygen partial pressure and is not influenced by the electrode morphology (Fig. 10). The calculated values range from a few mF cm^{-2}, under pure oxygen, to 0.1–0.7 F cm^{-2} at ($p_{O_2} \sim 10^{-4}$ atm). C_{LF} values do not
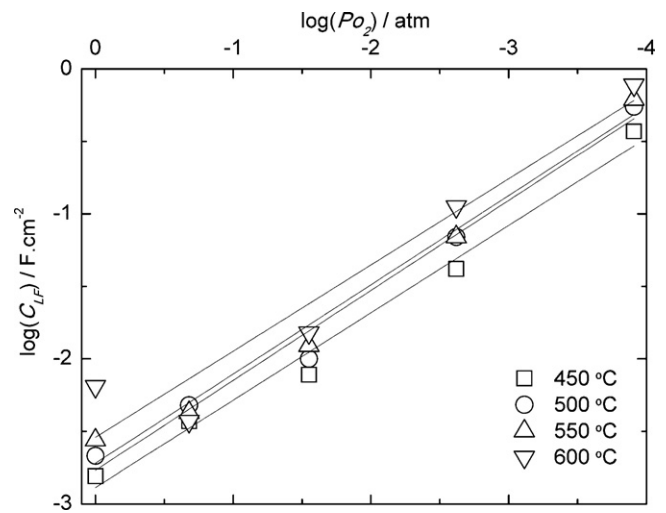
scale with the electrode thickness suggesting that mass transport limitations do not dominate the electrode impedance. This conclusion is in agreement with the previous assumption of a nearly constant effective electrode thickness. The high values of C_{LF} can be related to chemical capacitances [65], indicating a variation of the vacancy concentration in the electrode material as a function of oxygen pressure [66]. The observed increase of C_{LF} with temperature (Fig. 10) rather supports this assumption.

Due to the large contribution of the LF response to cathode polarization, the behavior of R_{pol} versus p_{O_2} is dictated by that of R_{LF} (Fig. 11), and similar behavior and n values were determined (Table 6). At $p_{O_2} > 10^{-2}$ atm, exponent values of the order

Table 5
Exponent n values for the p_{O_2} dependence of R_{LF} as a function of temperatures and oxygen pressure range, for different morphologies.

$T/°C$	$10^{-2} < p_{O_2} < 1$ atm			$10^{-4} < p_{O_2} < 10^{-2}$ atm		
	Dense	Cracked	Coral	Dense	Cracked	Coral
450	0.13	0.18	0.20	0.53	0.28	0.20
500	0.17	0.12	0.19	0.55	0.39	0.19
550	0.18	0.09	0.07	0.63	0.53	0.74
600	0.20	0.04	0.05	0.71	0.68	0.80

Table 6
Exponent n values for the p_{O_2} dependence of R_{pol} as a function of temperatures and oxygen pressure range, for different morphologies.

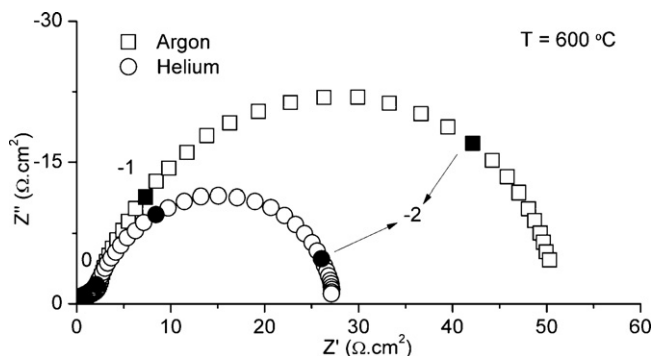| $T/°C$	$10^{-2} < p_{O_2} < 1$ atm			$10^{-4} < p_{O_2} < 10^{-2}$ atm		
	Dense	Cracked	Coral	Dense	Cracked	Coral
450	0.10	0.11	0.18	0.48	0.25	0.18
500	0.15	0.07	0.18	0.53	0.36	0.18
550	0.17	0.06	0.11	0.59	0.50	0.67
600	0.18	0.01	0.10	0.68	0.66	0.72

Fig. 12. Impedance diagrams recorded on dense sample at $600\,^{\circ}C$ and $p_{O_2} \sim 10^{-4}$ atm using Ar and He as gas carriers (OCP conditions). The numbers over the diagram indicate the logarithm of the measuring frequency.

of 0.2 indicate that surface exchange ($n = 0.25$) is rate-determining [67], irrespective of temperature and sample morphology. At $p_{O_2} < 10^{-2}$ atm and $T < 500\,^{\circ}C$, an n value of 0.5 was determined for the dense sample, which is commonly attributed to a dissociative adsorption limiting step [36,37]. Smaller n values were determined for cracked and coral cathodes in similar conditions, due to larger surface areas providing more active sites for oxygen adsorption.

At $T > 500\,^{\circ}C$ and in the low oxygen partial pressure range, n is intermediate between 0.5 and 1, indicating a mixed contribution of dissociative adsorption and gas-phase diffusion step [15,53], regardless of sample morphology. The gradual increase of n with temperature (Fig. 11), followed by a decrease of the corresponding activation energy (Table 4), indicates an increasing contribution of the gas-phase diffusion process. Such an evolution is not surprising since gas-phase concentration polarization is generally evidenced at high temperatures. At this stage, the results clearly indicate that below $500\,^{\circ}C$ the *LF* contribution is related to surface exchange and that above $500\,^{\circ}C$ and for oxygen partial pressures below 10^{-2} atm this process is kinetically mixed-controlled.

In order to precise the contribution of gas-phase diffusion processes, impedance measurements versus p_{O_2} were performed by replacing Argon for Helium as carrier gas (at constant flow rate). A decrease in R_{pol} values was observed by using Helium instead of Argon (Fig. 12), and the magnitude of the recorded decrease is most significant above $500\,^{\circ}C$ and under low oxygen pressures. Such behavior is explained by the higher diffusivity rate of oxygen in Helium relative to Argon, and further suggests the occurrence of a gas-phase diffusion process in the electrode reaction mechanism under these conditions. This effect is less pronounced in cracked and coral cathodes due to larger surface areas.

4. Conclusions

LSCF films with different morphologies were obtained by ESD. The cathodic behavior was characterized by impedance spectroscopy at intermediate temperature range ($450 < T < 600\,^{\circ}C$) under varying oxygen partial pressure conditions ($10^{-4} < p_{O_2} < 1$ atm). Impedance measurements showed that polarization resistance is determined by three common processes identified at high, medium and low frequency ranges, regardless of cathode morphology. On the basis of the temperature and oxygen partial pressure dependences of related electrical parameters, the processes described at high and intermediate frequency ranges were unequivocally identified as ionic transfer at the LSCF/CGO interface and ionic diffusion in the bulk of LSCF, respectively. The contribution described in the low frequency range, associated with oxygen exchange, was found to dominate the electrode impedance.

The oxygen reduction reaction in LSCF cathodes was evaluated. Under high oxygen pressures ($p_{O_2} > 10^{-2}$ atm), the LSCF cathodic reaction was found to be rate-limited by oxygen surface exchange. At lower oxygen pressures ($p_{O_2} < 10^{-2}$ atm), results were interpreted according to a limiting dissociative process coupled with gas-phase diffusion of oxygen, with increasing prevalence of the latter with increasing temperature. LSCF films were shown to maintain performance levels at p_{O_2} as low as 10^{-2} atm at temperatures above $550\,^{\circ}C$, which is advantageous for IT-SOFC applications.

References

[1] C.C. Kan, H.H. Kan, F.M. Van Assche, E.N. Armstrong, E.D. Wachsman, J. Electrochem. Soc. 155 (2008) B985–B993.
[2] S.P. Jiang, Solid State Ionics 146 (2002) 1–22.
[3] I. Yasuda, K. Ogasawara, M. Hishinuma, T. Kawada, M. Dokiya, Solid State Ionics 86–8 (1996) 1197–1201.
[4] L. Kindermann, D. Das, H. Nickel, Solid State Ionics 89 (1996) 215–220.
[5] H.Y. Tu, Y. Takeda, N. Imanishi, O. Yamamoto, Solid State Ionics 117 (1999) 277–281.
[6] B.C.H. Steele, Solid State Ionics 75 (1995) 157–165.
[7] L.W. Tai, M.M. Nasrallah, H.U. Anderson, D.M. Sparlin, S.R. Sehlin, Solid State Ionics 76 (1995) 273–283.
[8] B.C.H. Steele, Solid State Ionics 129 (2000) 95–110.
[9] D. Marinha, C. Rossignol, E. Djurado, J. Solid State Chem. 182 (2009) 1742–1748.
[10] D. Beckel, U.P. Muecke, T. Gyger, G. Florey, A. Infortuna, L.J. Gauckler, Solid State Ionics 178 (2007) 407–415.
[11] I. Taniguchi, R.C. van Landschoot, J. Schoonman, Solid State Ionics 156 (2003) 1–13.
[12] C.H. Chen, E.M. Kelder, P.J.J.M. vanderPut, J. Schoonman, J. Mater. Chem. 6 (1996) 765–771.
[13] A. Princivalle, D. Perednis, R. Neagu, E. Djurado, Chem. Mater. 16 (2004) 3733–3739.
[14] T. Abbasi, S.A. Abbasi, Renew. Sustain. Energy Rev. 15 (2011) 3034–3040.
[15] A. Esquirol, N.P. Brandon, J.A. Kilner, M. Mogensen, J. Electrochem. Soc. 151 (2004) A1847–A1855.
[16] Y.J. Leng, S.H. Chan, Q.L. Liu, Int. J. Hydrogen Energy 33 (2008) 3808–3817.
[17] X.Y. Lou, S.Z. Wang, Z. Liu, L. Yang, M.L. Liu, Solid State Ionics 180 (2009) 1285–1289.
[18] H.J. Hwang, M.B. Ji-Woong, L.A. Seunghun, E.A. Lee, J. Power Sources 145 (2005) 243–248.
[19] C.S. Hsu, B.H. Hwang, J. Electrochem. Soc. 153 (2006) A1478–A1483.
[20] J.M. Bae, B.C.H. Steele, Solid State Ionics 106 (1998) 247–253.
[21] J.W. Lee, Z. Liu, L. Yang, H. Abernathy, S.H. Choi, H.E. Kim, M.L. Liu, J. Power Sources 190 (2009) 307–310.
[22] D. Marinha, L. Dessemond, E. Djurado, ECS Trans. 28 (2010) 93–103.
[23] S.B. Adler, X.Y. Chen, J.R. Wilson, J. Catal. 245 (2007) 91–109.
[24] A. Ringuedé, J. Fouletier, Solid State Ionics 139 (2001) 167–177.
[25] Y. Takeda, R. Kanno, M. Noda, Y. Tomida, O. Yamamoto, J. Electrochem. Soc. 134 (1987) 2656–2661.
[26] H. Xiong, B.K. Lai, A.C. Johnson, S. Ramanathan, J. Power Sources 193 (2009) 589–592.
[27] Y. Tao, H. Nishino, S. Ashidate, H. Kokubo, M. Watanabe, H. Uchida, Electrochim. Acta 54 (2009) 3309–3315.
[28] V.C. Kournoutis, F. Tietz, S. Bebelis, Fuel Cells 9 (2009) 852–860.
[29] J. Chen, F.L. Liang, L.N. Liu, J. Pu, B. Chi, J. Li, Chin. J. Catal. 30 (2009) 131–136.
[30] C.S. Hsu, B.H. Hwang, Y. Xie, X. Zhang, J. Electrochem. Soc. 155 (2008) B1240–B1243.
[31] L. Baque, A. Caneiro, M.S. Moreno, A. Serquis, Electrochem. Commun. 10 (2008) 1905–1908.
[32] W.H. Kim, H.S. Song, J. Moon, H.W. Lee, Solid State Ionics 177 (2006) 3211–3216.
[33] A. Esquirol, J. Kilner, N. Brandon, Solid State Ionics 175 (2004) 63–67.
[34] E.P. Murray, M.J. Sever, S.A. Barnett, Solid State Ionics 148 (2002) 27–34.
[35] N. Grunbaum, L. Dessemond, J. Fouletier, F. Prado, A. Caneiro, Solid State Ionics 177 (2006) 907–913.
[36] N. Grunbaum, L. Dessemond, J. Fouletier, F. Prado, L. Mogni, A. Caneiro, Solid State Ionics 180 (2009) 1448–1452.
[37] Y.M. Kim, S.I. Pyun, J.S. Kim, G.J. Lee, J. Electrochem. Soc. 154 (2007) B802–B809.
[38] M. Prestat, A. Infortuna, S. Korrodi, S. Rey-Mermet, P. Muralt, L.J. Gauckler, J. Electroceram. 18 (2007) 111–120.
[39] L.W. Tai, M.M. Nasrallah, H.U. Anderson, D.M. Sparlin, S.R. Sehlin, Solid State Ionics 76 (1995) 259–271.
[40] J.B. Liu, A.C. Co, S. Paulson, V.I. Birss, Solid State Ionics 177 (2006) 377–387.
[41] M. Shah, S.A. Barnett, Solid State Ionics 179 (2008) 2059–2064.
[42] W.I. Zhou, Z.P. Shao, R. Ran, H.X. Gu, W.Q. Jin, N.P. Xu, J. Am. Ceram. Soc. 91 (2008) 1155–1162.
[43] J. Fleig, J. Maier, J. Electroceram. 1 (1997) 73–89.
[44] E.J. Abram, D.C. Sinclair, A.R. West, J. Electroceram. 7 (2001) 179–188.
[45] F.S. Baumann, J. Fleig, H.U. Habermeier, J. Maier, Solid State Ionics 177 (2006) 1071–1081.
[46] S.B. Adler, Chem. Rev. 104 (2004) 4791–4843.
[47] Y. Jiang, A.V. Virkar, F. Zhao, J. Electrochem. Soc. 148 (2001) A1091–A1099.

[48] F.S. Baumann, J. Fleig, G. Cristiani, B. Stuhlhofer, H.U. Habermeier, J. Maier, J. Electrochem. Soc. 154 (2007) B931–B941.
[49] M.J. Escudero, A. Aguadero, J.A. Alonso, L. Daza, J. Electroanal. Chem. 611 (2007) 107–116.
[50] H. Fukunaga, M. Koyama, N. Takahashi, C. Wen, K. Yamada, Solid State Ionics 132 (2000) 279–285.
[51] D.J. Chen, R. Ran, Z.P. Shao, J. Power Sources 195 (2010) 4667–4675.
[52] S.M. Liu, J.P. Suo, J.Z. Xiao, Int. J. Hydrogen Energy 33 (2008) 6322–6326.
[53] E.P. Murray, T. Tsai, S.A. Barnett, Solid State Ionics 110 (1998) 235–243.
[54] P. Hjalmarsson, M. Sogaard, M. Mogensen, Solid State Ionics 180 (2009) 1395–1405.
[55] S.P. Jiang, W. Wang, Y.D. Zhen, J. Power Sources 147 (2005) 1–7.
[56] A. Leonide, B. Ruger, A. Weber, W.A. Meulenberg, E. Ivers-Tiffée, J. Electrochem. Soc. 157 (2010) B234–B239.
[57] S. Lee, H.S. Song, S.H. Hyun, J. Kim, J. Moon, J. Power Sources 187 (2009) 74–79.
[58] A.V. Berenov, A. Atkinson, J.A. Kilner, E. Bucher, W. Sitte, Solid State Ionics 181 (2010) 819–826.
[59] B.C.H. Steele, J.M. Bae, Solid State Ionics 106 (1998) 255–261.
[60] S.J. Xu, W.J. Thomson, Chem. Eng. Sci. 54 (1999) 3839–3850.
[61] B.T. Dalslet, M. Sogaard, P.V. Hendriksen, Solid State Ionics 180 (2009) 1050–1060.
[62] S.B. Adler, J.A. Lane, B.C.H. Steele, J. Electrochem. Soc. 143 (1996) 3554–3564.
[63] D. Marinha, J. Hayd, L. Dessemond, E. Ivers-Tiffée, E. Djurado, J. Power Sources (2010).
[64] Z.Y. Jiang, C.R. Xia, F.L. Chen, Chin. J. Chem. Phys. 23 (2010) 217–225.
[65] J. Jamnik, J. Maier, PCCP 3 (2001) 1668–1678.
[66] T. Kawada, J. Suzuki, M. Sase, A. Kaimai, K. Yashiro, Y. Nigara, J. Mizusaki, K. Kawamura, H. Yugami, J. Electrochem. Soc. 149 (2002) E252–E259.
[67] S. Bebelis, N. Kotsionopoulos, A. Mai, F. Tietz, J. Appl. Electrochem. 37 (2007) 15–20.